Vision Research 51 (2011) 376–385

Contents lists available at ScienceDirect

Vision Research

journal homepage: www.elsevier.com/locate/visres

Retinal thinning in tree shrews with induced high myopia: Optical coherence tomography and histological assessment

Carla J. Abbott [a,1], Ulrike Grünert [a,b,1], Michael J. Pianta [a], Neville A. McBrien [a,*]

[a] Department of Optometry and Vision Sciences, The University of Melbourne, Parkville, Victoria 3010, Australia
[b] National Vision Research Institute of Australia, Carlton, Victoria 3053, Australia

ARTICLE INFO

Article history:
Received 28 July 2010
Received in revised form 3 December 2010
Available online 13 December 2010

Keywords:
Myopia
Retinal thinning
Optical coherence tomography
Tree shrew
Retinal cell density

ABSTRACT

This study determined retinal thinning in a mammalian model of high myopia using optical coherence tomography (OCT) and histological sections from the same retinal tissue. High myopia was induced in three tree shrews (*Tupaia belangeri*) by deprivation of form vision via lid suture of one eye, with the other eye a control. Ocular biometry data was obtained by Ascan ultrasonography, keratometry and retinoscopy. The Zeiss StratusOCT was used to obtain Bscans *in vivo* across the retina. Subsequently, eyes were enucleated and retinas fixed, dehydrated, embedded and sectioned. Treated eyes developed a high degree of axial myopia (−15.9 ± 2.3 D; $n = 3$). The OCT analysis showed that in myopic eyes the nasal retina thinned more than the temporal retina relative to the disc ($p = 0.005$). Histology showed that the retinas in the myopic eyes comprise all layers but were thinner than the retinas in normal and control eyes. Detailed thickness measurements in corresponding locations of myopic and control eyes in superior nasal retina using longitudinal reflectivity profiles from OCT and semithin vertical histological sections showed the percentage of retinal thinning in the myopic eyes was similar between methods (OCT 15.34 ± 5.69%; histology 17.61 ± 3.02%; $p = 0.10$). Analysis of retinal layers revealed that the inner plexiform, inner nuclear and outer plexiform layers thin the most. Cell density measurements showed all neuronal cell types are involved in retinal thinning. The results indicate that *in vivo* OCT measurements can accurately detect retinal thinning in high myopia.

1. Introduction

Myopia has a high prevalence in the human population, with some degree of myopia present in 20–42% of individuals in Australia, Europe and North America respectively and with a higher prevalence of 60–80% reported in South East Asian populations (Fledelius, 1988; Goh & Lam, 1994; Lin et al., 1999; Vitale, Sperduto, & Ferris, 2009; Wensor, McCarty, & Taylor, 1999; Wu et al., 2001). Low to moderate degrees of myopia represent a relatively minor inconvenience in the developed world, as blurred distance vision can be corrected using spectacles, contact lenses or refractive surgery. High degrees of myopia, typically classed as in excess of 5 or 6 dioptres (D) (Curtin, 1985; Kempen et al., 2004), while also correctable using the above measures, are of major concern due to the incidence of myopia related pathology, since the risks of retinal atrophy, chorioretinal degeneration and retinal detachment are significantly increased (Celorio & Pruett, 1991; Yannuzzi, Sorenson, et al., 1993). Up to 70% of myopes over 6 D are reported to have sight threatening ocular pathology (Chiang et al., 1993; Grossniklaus & Green, 1992). Prevalence studies indicate that some 12–17% of all myopes have myopia greater than 5 D, resulting in a prevalence of high myopia in the general population of approximately 2–3% in Western developed nations (Kempen et al., 2004), and significantly higher in South East Asian populations (Lin et al., 1999; Wu et al., 2001). High myopia is thus amongst the leading causes of registered blindness and partial sight in the populations of the developed world, particularly in the working population (Chiang et al., 1993; Grey, Burns-Cox, & Hughes, 1989; Maruo, Ikebukuro, Kawanabe, & Kubota, 1991; Rosenberg & Klie, 1996).

High myopia is invariably due to excessive elongation of the eye. High myopes are at greater risk of developing sight threatening pathology of the retina and choroid, primarily due to the increased mechanical stresses placed on these tissues in elongated eyes (David, Smye, Dabbs, & James, 1998). Clinical reports (Curtin, 1985; Curtin & Karlin, 1971; Tokoro, 1998) of chorioretinal atrophy in the fundus of eyes with high myopia and histological studies (Curtin, 1985; McBrien, Moghaddam, Cottriall, Leech, & Cornell, 1995; Yanoff & Fine, 2002), indicate that myopia is associated with

* Corresponding author. Fax: +61 3 9349 7474.
E-mail addresses: carla.abbott@sydney.edu.au (C.J. Abbott), ulrike.grunert@sydney.edu.au (U. Grünert), mjp@unimelb.edu.au (M.J. Pianta), nmcbrien@unimelb.edu.au (N.A. McBrien).
[1] Present address: Save Sight Institute, C09 Clinical Ophthalmology and Eye Health, GPO Box 4337, The University of Sydney, NSW 2006, Australia.

0042-6989/$ - see front matter © 2010 Elsevier Ltd. All rights reserved.
doi:10.1016/j.visres.2010.12.005

thinning of the retina. Additionally, *in vivo* measurements of retinal thickness in human high myopia with optical coherence tomography (OCT) (Hee et al., 1995; Huang, Swanson, et al., 1991) and the retinal thickness analyzer (Kremser, Troger, Baltaci, Kralinger, & Kieselbach, 1999) have identified retinal thinning at the posterior pole of the eye (Choi & Lee, 2006; Lam et al., 2007; Leung, Mohamed, et al., 2006; Liew, Gilbert, Spector, Marshall, & Hammond, 2007; Lim et al., 2005; Luo, Gazzard, et al., 2006; Wolsley, Saunders, Silvestri, & Anderson, 2008; Wu et al., 2008). It remains unknown whether thinning occurs equally in all retinal layers, although one OCT study in human suggests it occurs more in the middle to inner retina (outer plexiform layer to nerve fiber layer) (Wolsley et al., 2008). No study to date has directly compared *in vivo* with histological measures of retinal thinning in myopia. However, retinal thickness measurements in normal rabbit, monkey and tree shrew (Abbott, McBrien, Grünert, & Pianta, 2009; Anger et al., 2004; Ge, Luo, & Guo, 1999) using both OCT and histological methods show good agreement.

The aim of the present study is to quantify changes in retinal thickness (in total and across layers) in an animal model of axial myopia. The tree shrew is a commonly used mammalian model of axial myopia development. Tree shrews have a similar ocular structure to humans and their developmental ocular growth responses are well documented (McBrien & Gentle, 2003; McBrien & Norton, 1992). The percentage of retinal thinning in axial high myopia is determined and compared between OCT (*in vivo*) and histological (*in vitro*) methods. These results help to determine the accuracy of OCT as an *in vivo* tool for assessing changes in retinal thickness in myopia.

2. Materials and methods

2.1. Animal model of myopia

Three maternally reared tree shrews (*Tupaia belangeri*) from our breeding colony (TS1, TS2 and TS3) were used. Animals were maintained on a 15:9 h (light:dark) cycle, with light levels at the cage floor approximately 250 lux. Food and water were available *ad libitum*.

Fifteen to twenty days after eye opening, animals were anaesthetized with a mixture of ketamine (90 mg/kg) and xylazine (10 mg/kg) given intramuscularly. The lids of one eye were then sutured, as previously described (McBrien & Norton, 1992). In order to induce high levels of axial myopia, animals experienced between 19 and 21 months of form deprivation (TS1 19.7 months, TS2 20.6 months, TS3 19.0 months). Lid suture is the only validated method available for the long term deprivation of form vision in the tree shrew and form deprivation is a well characterized method of inducing axial myopia (Marsh-Tootle & Norton, 1989; McBrien & Norton, 1992; Sherman, Norton, & Casagrande, 1977). The alternative method of inducing myopia using negative powered lenses in a head mounted goggle (Siegwart & Norton, 1994) cannot be used for experimental periods longer than about 8 weeks (Metlapally & McBrien, 2008).

After the prescribed period of form deprivation, lids were reopened in order to conduct biometric measures and imaging procedures. Pupils were dilated (1% tropicamide; Alcon Australia) and the cornea anaesthetized (0.5% proxymetacaine hydrochloride, Alcaine; Alcon Australia). Ascan ultrasonography (10 MHz focused transducer; LeCroy 9400 digital storage oscilloscope, Geneva, Switzerland) was used to obtain axial dimensions of the ocular components. Corneal curvature was measured using a modified Bausch & Lomb one position keratometer. Cycloplegic refractive error was measured using a streak retinoscope (Keeler). Measures were taken on both eyes of each animal. Artificial tears (Artificial Tears; CIBA Vision Australia) were applied regularly to prevent corneal desiccation during retinal imaging. A bite bar stabilized the animal's head (Norton & McBrien, 1992) and eyelids were retracted with a custom made speculum. Further details of the ocular biometry methodology have been described elsewhere (McBrien, Moghaddam, & Reeder, 1993; Norton & McBrien, 1992). All animals were treated in accordance with the ARVO statement for the Use of Animals in Ophthalmic and Vision Research and institutional ethics approval was obtained.

2.2. Optical coherence tomography and image processing

A third-generation OCT system (StratusOCT, Model number 3000; Carl Zeiss Ophthalmic Systems, Dublin, California, USA) was used to acquire Bscans and custom quantitative analysis (MATLAB 7; MathWorks, Natick, MA) was performed as described previously (Abbott et al., 2009). Briefly, each Bscan was registered relative to the optic disc and blood vessels seen in its corresponding fundus photo, and coregistered relative to all scans to create an accurate *in vivo* ocular fundus map (Fig. 1). Individual longitudinal reflectivity profiles (LRPs) were assigned to bins (100 μm × 100 μm in area) based on their registered position. The LRPs in each bin were aligned, averaged and smoothed to create a mean LRP for the area of retina encompassed by the bin. Axial length measures were used to correct the lateral OCT Bscan length for the tree shrew eyes based on retinal magnification factor calculations (Wakitani et al., 2003).

2.3. Histological processing

Following the *in vivo* procedures animals were administered a lethal dose of sodium pentobarbital (120 mg/kg). Full details of the histological processing protocol and lateral shrinkage calculations have been previously described (Abbott et al., 2009). Briefly, the eyes were enucleated and the posterior eyecup was immersion fixed in 2.5% glutaraldehyde and 1% paraformaldehyde in 0.1 M phosphate buffer, pH 7.2. The retina was dissected, cut into quadrants and kept flat during dehydration and embedding. The mean (±SD) lateral shrinkage due to tissue dehydration was 22.96 (±0.77)% in the control eyes (n = 3 retinas) and 23.53 (±0.99)% in the myopic eyes (n = 3 retinas). These values are not significantly different (p = 0.475; t-test) and are within the range of reported values (8–29%) (Abbott et al., 2009; Adams, Perez, & Hawthorne, 1974; Curcio, Packer, & Kalina, 1987; Kolb & Wang, 1985; Ogden, 1975; Perry & Cowey, 1985; Reymond, 1985; Steinberg, Reid, & Lacy, 1973). Serial vertical semithin (1 μm) sections were cut on a Reichert ultramicrotome, stained with toluidine blue and micrographs were taken with a Zeiss Axioplan 2 microscope. Axial shrinkage estimates were determined as previously described (Abbott et al., 2009).

2.4. Selection of retinal locations for analysis

In vivo retinal maps were created for the three myopic and three control eyes (Fig. 1) as previously described (Abbott et al., 2009). Subsequently, a systematic analysis of all retinal quadrants (superior nasal, inferior nasal, superior temporal and inferior temporal with respect to the optic disc) was carried out using the OCT data. A square grid of nine locations (i.e. 100 μm × 100 μm bins) in each retinal quadrant out to 18° from the optic disc center, separated from their neighboring locations by 500 μm, was overlaid on each retinal map to select matching locations. Shifts of these locations up to 100 μm were occasionally required to avoid blood vessels. Thinning was calculated for each location in the myopic eye relative to the control and averaged (±SD) for each quadrant. The superior nasal quadrant showed the smallest standard deviation across animals and the greatest thinning (see Section 3) so was used for a more detailed analysis to investigate potential differences in thinning between measurement methods and retinal layers.

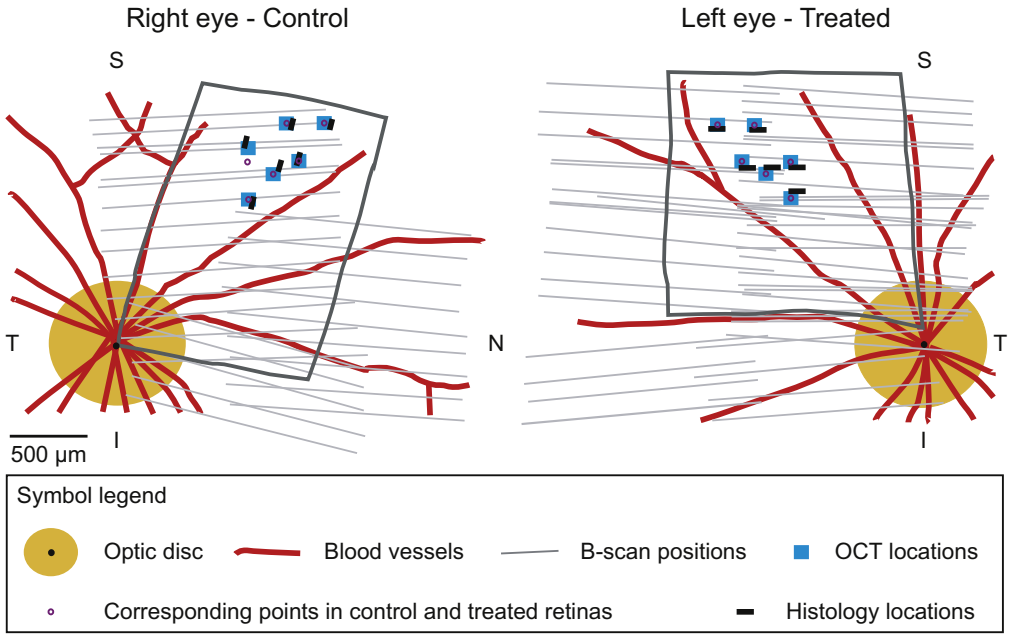

Fig. 1. Example of retinal maps of the control and treated eye superior nasal quadrants (TS2) to show the positions of analyzed retinal locations. The blood vessels and the optic disc were used as landmarks to align the OCT and histology data. Points in the control and treated eyes corresponding for retinal eccentricity were identified. OCT and histology locations within 100 μm of these identified points were selected for analysis. For further information about the method of reconstructing the retinal maps, refer to Abbott et al. (2009). Grey rectangles indicate regions cut into vertical sections. Refer to the symbol legend for other symbol information. Abbreviations: superior retina (S), nasal retina (N), inferior retina (I), temporal retina (T).

For this detailed analysis, LRP and histology pairs were chosen from equivalent locations (±100 μm) (Fig. 1) as previously described (Abbott et al., 2009). Exact positions and dimensions of the vertical sections were matched to the *in vivo* map, after accounting for lateral shrinkage due to dehydration during tissue processing. Eccentricity and area measurements are presented in predehydration units. The maps were additionally used to ensure that pairings from treated and control eyes within each animal were from equivalent retinal locations (±100 μm). When selecting OCT bins for the detailed analysis the following criteria were used. Retinal locations near inner retinal blood vessels were avoided due to shadowing of the OCT signal. A sampling density of at least three Bscans per bin was required to achieve a signal to noise ratio that enabled the features within each mean LRP to be reliably identified. When selecting retinal histology for analysis, sections with artifacts/disturbances were avoided. Fifteen paired retinal locations were analyzed from comparable eccentricities, 1.6–2.7 mm (i.e. 16–27°) superior nasal to the center of the optic disc (e.g. Fig. 1). There were six locations from each of TS1 and TS2. In TS3 only three locations were analyzed because it was not possible to obtain more matching locations using the criteria outlined above. The data from the 15 independent locations were pooled and averaged for each tree shrew, then total mean retinal thickness and thinning values were calculated where the standard deviation represents the variation across animals.

A further 24 locations were selected from the OCT maps of two normal tree shrews (aged 9 and 26 months) used in a previous study (Abbott et al., 2009). In these tree shrews both eyes had undergone normal binocular visual development. Six retinal locations were selected from each of the four normal eyes, with eccentricities that ranged from 1.8 mm to 2.7 mm superior nasal from the center of the optic disc.

2.5. Interpretation of the OCT signal

The present study uses the previously defined interpretation of the OCT signal in tree shrew (Abbott et al., 2009) as a basis for the *in vivo* retinal thickness measurements. Briefly, nerve fiber, plexiform layers and retinal pigment epithelium are highly reflective, whereas inner and outer nuclear layers are less reflective. The innermost peak in reflectivity corresponds to the nerve fiber layer and the ganglion cell layer. The outer highly reflective peak represents the inner and outer segments of the photoreceptors, the retinal pigment epithelium and the choriocapillaris. For detailed discussion on the comparison of the OCT interpretation in tree shrew and human, see Abbott et al. (2009).

2.6. Retinal thickness measurements

To measure the retinal thickness from the mean LRP, a custom MATLAB program was employed to aid identification of the boundaries corresponding to retinal layers (Abbott et al., 2009). Each thickness measurement was made in pixels and then converted to micrometers based on the number of pixels within the depth of the scan (1024 pixels over 2 mm for the StratusOCT). For the corresponding histology locations, thicknesses in micrometers were measured on a digital micrograph (width 100 μm) taken with a 40× oil immersion objective by manually identifying the average position of the retinal layer boundaries across the section, then measuring the distances between the boundaries.

Table 1
Ocular biometry measures for each tree shrew (TS).

Ocular biometry measure	Difference (T − C)		
	TS1	TS2	TS3
Refractive error (D)	−18.3 ± 0.5	−13.7 ± 0.7	−15.8 ± 1.3
Corneal curvature (D)	−2.50 ± 0.06	−3.40 ± 0.25	−3.68 ± 0.35
Anterior chamber depth (mm)	−0.11 ± 0.02	−0.11 ± 0.03	−0.06 ± 0.01
Lens thickness (mm)	−0.05 ± 0.01	−0.01 ± 0.01	−0.03 ± 0.01
Vitreous chamber depth (mm)	+0.82 ± 0.08	+0.49 ± 0.03	+0.81 ± 0.08
Axial length (mm)	+0.66 ± 0.08	+0.38 ± 0.05	+0.72 ± 0.08

Measurements are expressed as the difference (mean ± SD) between treated (T) and control (C) eyes. The number of measurements averaged for each eye are: refractive error $n = 2$, corneal curvature $n = 3$, anterior chamber depth, lens thickness, vitreous chamber depth, axial length $n = 6$.

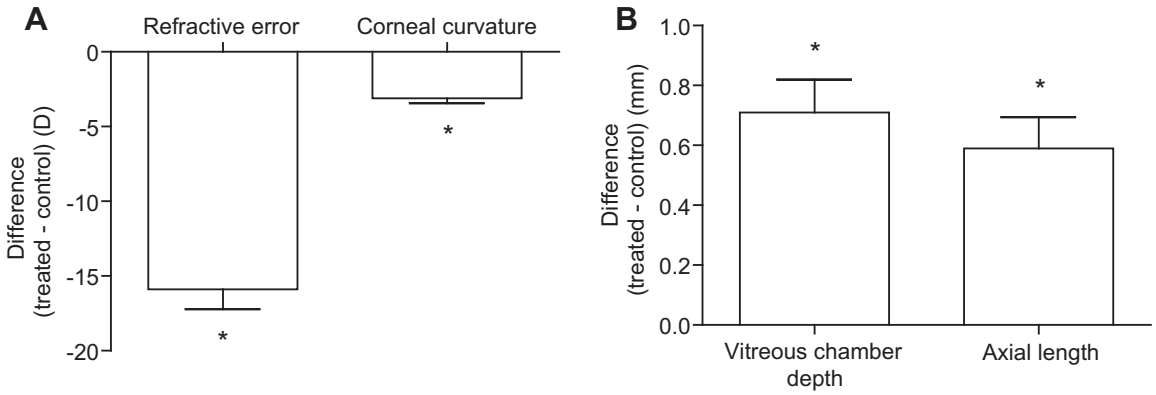

Fig. 2. Biometry results expressed as the difference (mean ± SEM) between eyes (treated–control). Data was calculated for each tree shrew separately, then averaged so that the SEM represents variation across animals ($n = 3$). (A) Difference in ocular refraction and corneal curvature in dioptres. (B) Difference in vitreous chamber depth and axial length in millimeters. The results show that axial myopia has developed in the treated eyes. One sample t-test for significant difference from zero: refractive error, $p = 0.007$; corneal curvature, $p = 0.012$; vitreous chamber depth, $p = 0.023$; axial length, $p = 0.030$. *indicates $p < 0.05$.

Table 2
OCT quadrant analysis of retinal thinning.

Retinal quadrant relative to optic disc	Retinal thinning (%)	p
Superior nasal	13.7 ± 2.5	0.011
Inferior nasal	13.3 ± 3.4	0.021
Superior temporal	7.3 ± 5.0	0.127
Inferior temporal	7.6 ± 3.2	0.053

The percentage of retinal thinning (mean ± SD) in the myopic eyes as calculated from Eq. (1). $n = 9$ locations per quadrant and $n = 3$ animals. p-Values calculated with one sample t-test for significant difference from zero.

Total retinal thickness is defined as the distance between the inner limiting membrane and the retinal pigment epithelium/choriocapillaris boundary. Retinal thickness was also determined for four layer 'zones', of which the first three zones have been defined previously (Abbott et al., 2009). Zone 1 represents the retinal nerve fiber and ganglion cell layers. Zone 2 represents the inner plexiform layer and amacrine cells of the inner nuclear layer. Zone 3 represents the Müller, bipolar and horizontal cells of the inner nuclear layer and the outer plexiform layer. The definition of zone 4 is also based on a previous interpretation and represents the outer nuclear layer, inner and outer segments of the photoreceptors and the retinal pigment epithelium.

2.7. Retinal thinning calculations

Retinal thinning due to myopia was calculated from the retinal thickness measures relative to the control thickness as a normalized percentage:

$$\text{Retinal thinning } (\%) = 100\left(\frac{T_C - T_T}{T_C}\right) \quad (1)$$

where T_C is control eye retinal thickness and T_T is treated eye retinal thickness, and control and treated retinal locations are from corresponding eccentricities. The percentage thinning detected in each retinal zone (U_i) for $i = 1, 2, 3$ and 4, as calculated from Eq. (1), can also be expressed as a proportion of the sum of the thinning from all zones (P_i) for each animal:

$$P_i = \frac{U_i}{\sum_i U_i} \quad (2)$$

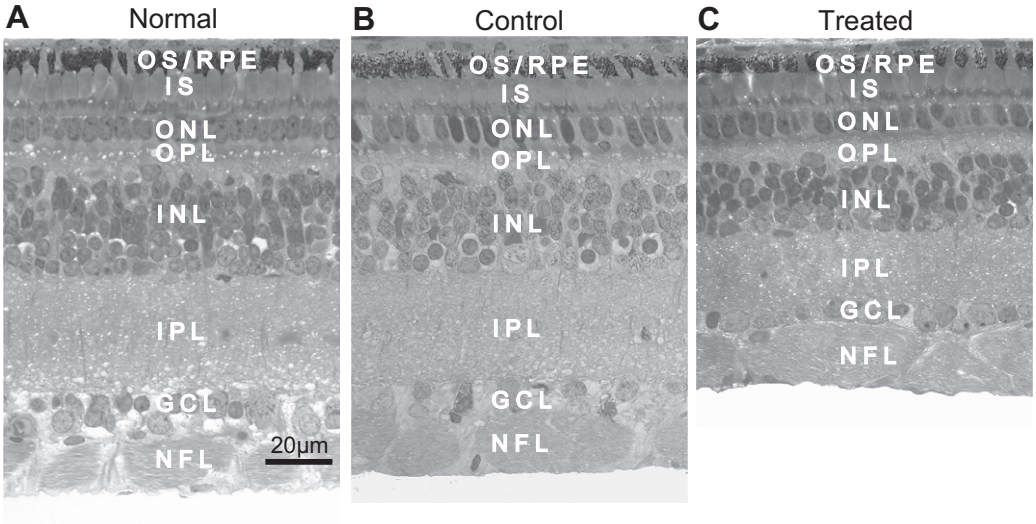

Fig. 3. Micrographs of Toluidine blue stained vertical sections through (A) retina from a normal tree shrew (Abbott et al., 2009), (B) retina from the control eye of TS2 and (C) retina from the treated eye of TS2. All micrographs are from equivalent locations: normal 2.5 mm, control 2.3 mm and treated 2.3 mm superior nasal to the optic disc. The treated retina is thinner than the normal and control retinas. Note that the outer segments of the photoreceptors are fully ensconced within the retinal pigment epithelium, so they are considered a combined layer. Abbreviations: nerve fiber layer (NFL), ganglion cell layer (GCL), inner plexiform layer (IPL), inner nuclear layer (INL), outer plexiform layer (OPL), inner (IS) and outer (OS) segments of the photoreceptors, retinal pigment epithelium (RPE).

2.8. Cell density calculations

2.8.1. Areal density

Areal cell density (D_A, cells/mm^2) was determined by cell counts for one location (size = 560 μm × 560 μm; position = 2.7 mm superior nasal to the center of the optic disc) matched in control and myopic eyes of one animal (TS1). An *a priori* power analysis showed that 48 retinal samples were required to detect a 20% difference in cell density ($\alpha = 0.05$) with a power of 0.9.

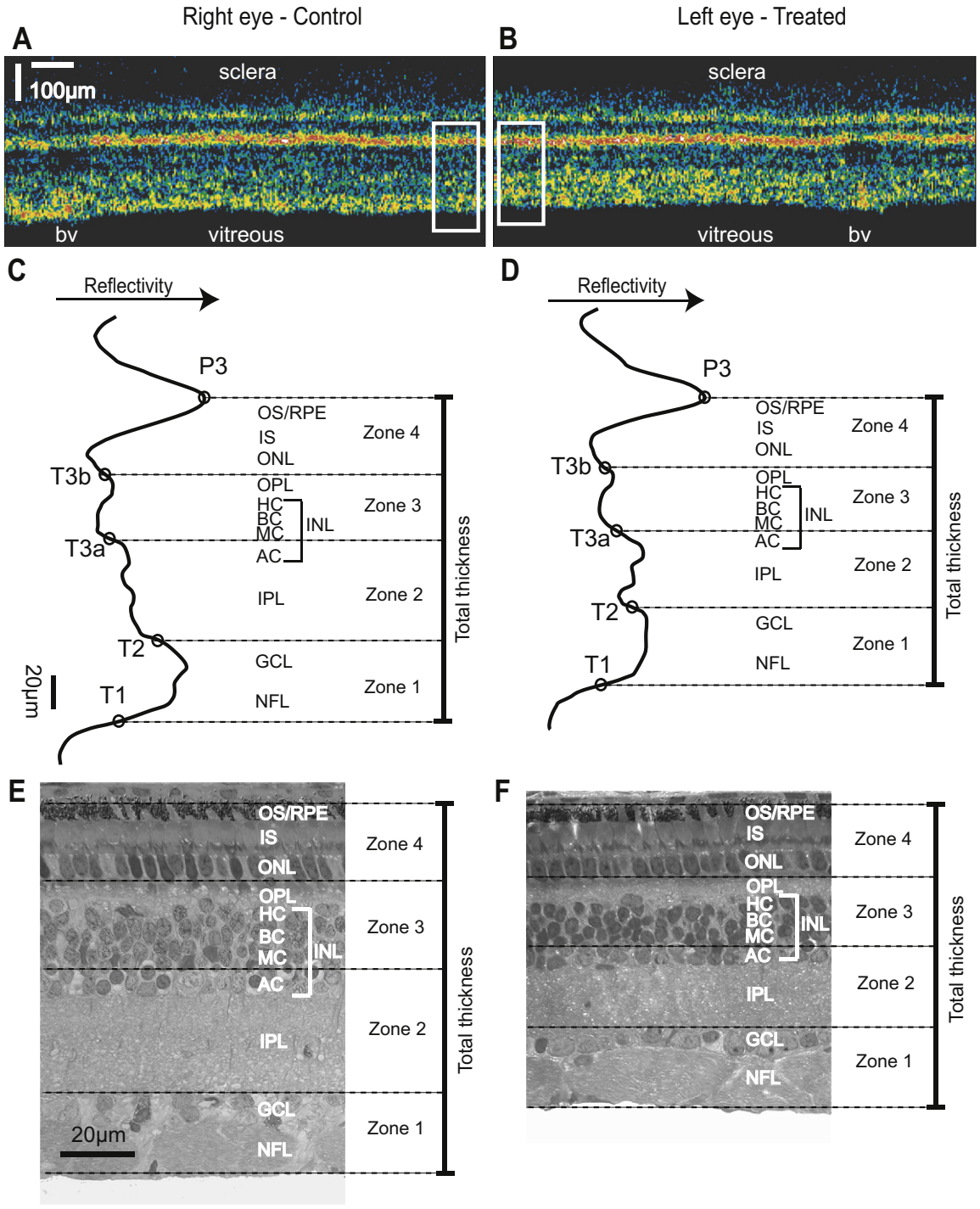

Fig. 4. An example of the method used to measure retinal thickness using OCT and histology. This example is from 2.3 mm superior nasal to the optic disc in TS2. (A and B) OCT Bscans in control and treated eyes. In a printed greyscale version of this figure, white represents high reflectivity and black represents low reflectivity, while in the online colour version, white and red represent high reflectivity and blue and black represent low reflectivity. (C and D) Mean longitudinal reflectivity profiles (LRP) derived from locations indicated by the rectangles in A and B. The four zones defined here were determined from LRP transitions (T) as described previously (Abbott et al., 2009). (E and F) Vertical histology sections corresponding to the LRPs in C and D. The total thickness was measured from the inner limiting membrane (ILM) to the retinal pigment epithelium (RPE)/choriocapillaris boundary. Zone 1 = ILM, nerve fiber layer (NFL) and ganglion cell layer (GCL). Zone 2 = inner plexiform layer (IPL) and amacrine cell (AC) somas of the inner nuclear layer (INL). Zone 3 = Müller cell (MC), bipolar cell (BC) and horizontal cell (HC) somas of the INL and outer plexiform layer (OPL). Zone 4 = inner (IS) and outer (OS) segments of the photoreceptors and RPE. In both methods the control retina is thicker than the treated retina, indicating that retinal thinning has occurred in the eye with high myopia.

The areal cell density was calculated using cell counting with the method of recursive reconstruction, which is fully described by Rose and Rohrlich (1988). Briefly, a computer attached camera lucida system (Goodchild & Martin, 1998; Halasz & Martin, 1984; Wilder, Grünert, Lee, & Martin, 1996) was used to draw the position and size of cell soma profiles and the position of laminar boundaries in 102 retinal samples (each 66 μm long) taken from twelve vertical sections (560 μm long) using a 100× oil immersion objective. Sections were spaced at least 10 μm apart to ensure independence. For a sample of cells for each cell population, the area of the neuronal profile was measured and the equivalent area diameter calculated. The recursive reconstruction method enables calculation of the ratio between the number of soma profiles in a section and the number of cells which give rise to the profiles. This number is used as a correction factor to convert the total number of profiles counted to the number of actual cells. There was no significant difference in the correction factors between control and treated eyes for each cell type (bipolar and horizontal cells, $p = 0.400$; rods and cones, $p = 0.700$; amacrine cells, $p = 0.658$; Müller cells, $p = 0.376$; ganglion cells, $p = 1.000$; Mann Whitney non-parametric test for independent samples), so they were combined and averaged. Taking into account the area of the region where profiles were counted allows the areal density to be calculated. The recursive reconstruction method does not assume size homogeneity in the target population, which is an advantage over alternative cell counting methods (Rose & Rohrlich, 1988).

Amacrine, Müller, bipolar and horizontal cells were distinguished by their morphological appearance and location within the inner nuclear layer (Cao, Murphy, & Petry, 1999; Ochs, Mayhew, & Knabe, 2000; Reichenbach et al., 1995). Müller cell somas are more polygonal than either amacrine or bipolar cells somas (see Fig. 2B of Abbott et al. (2009)). Amacrine cells are located on the inner side of the close knit Müller cell sublayer and bipolar cells on the outer side (Abbott et al., 2009). Bipolar and horizontal cells were not distinguished from each other since the horizontal cell population was small.

2.8.2. Volumetric density

The volumetric cell density (D_V, cells/mm^3) was determined for each cell type as follows:

$$D_V = \frac{D_A}{T_S} \tag{3}$$

where T_S is the total layer thickness (mm). Layer thickness was measured in the center of each section using the measuring tool in Zeiss Axiovision 4.2 software, and then averaged.

3. Results

3.1. Refractive and ocular biometry

The biometry measures are expressed as the difference between treated and control eyes for each animal and then averaged across the animals. All tree shrews showed high levels of myopia in the lid sutured eye compared to the control eye (mean ± SD = −15.9 ± 2.3 D; $p = 0.007$; one sample t-test) (Table 1 and Fig. 2). The cornea was flatter in the lid sutured eyes compared to the control eyes (−3.1 ± 0.6 D; $p = 0.012$; one sample t-test). The vitreous chamber depth of lid sutured eyes was on average 28 ± 7% longer than in control eyes (0.71 ± 0.19 mm; $p = 0.023$; one sample t-test) with a concomitant increase in the axial length (0.59 ± 0.18 mm; $p = 0.030$; one sample t-test).

3.2. Retinal morphology

Histological sections show that the retinas in the myopic eyes comprise all layers, but have a reduced thickness compared to both control and normal eyes (Fig. 3). The retinas of the three control eyes looked comparable to those of normal eyes except for a region near the optic disc where nonmechanical disturbances (i.e. not related to processing artifacts) were found. These disturbances were not seen in the myopic eyes or in the normal eyes (Abbott et al., 2009), and predominantly affected the photoreceptors including swelling, degeneration and thickening of inner segments, and degeneration and orientation changes in the somas. Retinal pigment epithelium folding and migration, as well as soma migration from the three nuclear layers into the plexiform layers, were also occasionally seen (not shown). These retinal changes could not be detected in the OCT Bscans. Only retinal locations that were unaffected by disturbances were selected for the detailed retinal thinning analysis and the cell density analysis, thus providing confidence that the results are representative of changes due only to myopia.

3.3. Total retinal thinning

The initial OCT analysis showed the retinal quadrants were subject to thinning in the myopic eyes (Table 2). The nasal retina underwent greater thinning than the temporal retina ($p = 0.005$; paired t-test). Retinal thickness in the superior nasal quadrant had the lowest variability between animals and the highest amount of thinning so was thus chosen for the detailed analysis.

Table 3
Retinal thickness and retinal thinning in the superior nasal quadrant.

Zone	Eye	Retinal thickness		Retinal thinning	
		OCT (μm)	Histology (μm)	OCT (%)	Histology (%)
Total	Normal	213.78 ± 9.05	Not determined		
	Control	210.07 ± 19.48	136.95 ± 8.84		
	Treated	177.33 ± 11.50	112.82 ± 10.35	15.34 ± 5.69	17.61 ± 3.02
Zone 1	Control	60.07 ± 12.25	36.38 ± 8.86		
	Treated	50.58 ± 5.92	32.50 ± 8.41	14.44 ± 7.73	10.01 ± 9.69
Zone 2	Control	63.06 ± 3.63	42.31 ± 3.51		
	Treated	50.62 ± 3.26	31.55 ± 4.84	19.64 ± 5.66	25.39 ± 5.74
Zone 3	Control	43.72 ± 2.48	30.10 ± 2.45		
	Treated	36.28 ± 1.70	23.78 ± 2.34	16.78 ± 8.68	20.85 ± 5.65
Zone 4	Control	43.22 ± 2.86	28.16 ± 0.53		
	Treated	39.85 ± 2.49	25.00 ± 0.11	7.73 ± 0.95	11.11 ± 1.97

All results are shown as mean ± SD. Data was calculated for each tree shrew separately, then averaged so the standard deviation represents the variation across animals ($n = 3$). Retinal thinning was calculated from Eq. (1) and is expressed as a normalized percentage. Control total retinal thickness is not significantly different to the normal total retinal thickness (unpaired t-test; $p = 0.74$).

An example of the detailed retinal thickness measurement using OCT and histology is shown in Fig. 4. The total retinal thickness of the control eyes (mean ± SD = 210 ± 19 μm) was comparable to that of the normal eyes (213 ± 11 μm) ($p = 0.74$; unpaired t-test) measured with OCT (Table 3). The total retinal thinning in the myopic eyes normalized to the control eyes was 15.3 ± 5.7% by the OCT method ($p < 0.001$; one sample t-test) (Fig. 5A and Table 3). Retinal thinning determined by the histology method was 17.6 ± 3.0% ($p < 0.001$; one sample t-test). Thus, the results for the two methods were comparable ($p = 0.10$; paired t-test).

3.4. Differential thinning of retinal layers and axial shrinkage

Retinal thinning was determined for four retinal zones (Fig. 4). The amount of retinal thinning within each zone of retina was equivalent between the OCT and histology methods as shown in Fig. 5A (zone 1, $p = 0.468$; zone 2, $p = 0.101$; zone 3, $p = 0.246$; zone 4, $p = 0.081$; paired t-test). The proportion each zone contributed to the total retinal thinning accounts for variations in the amount of thinning between animals and is shown in Fig. 5B (OCT) and Fig. 5C (histology). Zones 2 and 3 contribute the most to total thinning for both methods (Fig. 5), suggesting the inner plexiform layer (zone 2) and the inner nuclear layer and/or outer plexiform layer (zone 3) thin the most in axial myopia.

Axial shrinkage of the histology sections was equivalent between control and myopic eyes for total shrinkage (control 34.6 ± 4.9%; myopic 36.2 ± 6.8%; $p = 0.686$; paired t-test) and for individual zone shrinkage (zone 1, $p = 0.586$; zone 2, $p = 0.500$; zone 3, $p = 0.689$; zone 4, $p = 0.194$; paired t-test). Hence, the results for the control and myopic eyes were combined and averaged to compare axial shrinkage between zones. Axial shrinkage shows some variability, but was found to be equivalent between zones (zone 1 = 38.0 ± 7.3%; zone 2 = 34.9 ± 10.3%; zone 3 = 32.6 ± 7.5%; zone 4 = 35.9 ± 4.0%; one way ANOVA, $p = 0.661$). Furthermore, each zone was within the 95% confidence interval (24.6–46.2%) of the total axial shrinkage (mean = 35.4%), indicating shrinkage is close to linear. However, previous results (Abbott et al., 2009) show that a small amount of non-linear axial shrinkage does occur due to variations in microstructure and water content. The linearity of shrinkage will not affect the results in this study as it is equivalent between control and myopic eyes within zones.

3.5. Cell density measurements

The retina from the myopic eye of TS1 showed a decrease in areal cell density for all cell types (bipolar and horizontal cells, $p < 0.001$; rods and cones, $p = 0.033$; amacrine cells, $p < 0.001$; ganglion cells, $p < 0.001$; unpaired t-test) except Müller cells ($p = 0.292$; unpaired t-test) (Fig. 6A). The volumetric density calculation takes into account the differences in cell layer thicknesses between myopic and control eyes. There were no differences in volumetric cell density between myopic and control eyes for all cell types (rods and cones, $p = 0.555$; amacrine cells, $p = 0.086$; Müller cells, $p = 0.581$; ganglion cells, $p = 0.542$; unpaired t-test) except the bipolar and horizontal cell group ($p = 0.028$; unpaired t-test) (Fig. 6B).

4. Discussion

4.1. Refractive and biometric results

High myopia due to axial elongation of the vitreous chamber occurred in all form-deprived eyes. Refractive and ocular biometry findings are in agreement with previous studies (e.g. Marsh-Tootle & Norton, 1989; McBrien & Norton, 1992). As retinal thinning in human high myopia is thought to be due to axial elongation of the globe causing retinal stretch (Wu et al., 2008), and since our biometric findings replicate human axial myopia, it is likely our findings regarding retinal thinning in tree shrew should translate to human.

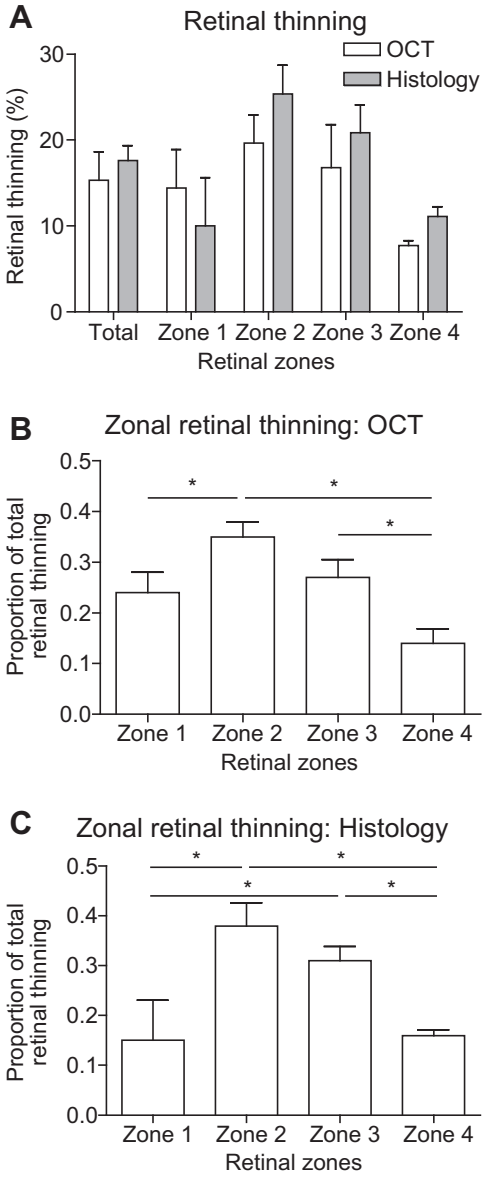

Fig. 5. Results of retinal thinning in the treated eye (mean ± SEM). Thinning was calculated for each tree shrew separately, then results were combined and averaged so that the SEM shown represents the variation across animals ($n = 3$). (A) Thinning in the treated eye as calculated with Eq. (1). See Fig. 4 for the definition of zone boundaries. There is no difference in retinal thinning between OCT and histology methods in total or within any of the zones (total, $p = 0.097$; zone 1, $p = 0.468$; zone 2, $p = 0.101$; zone 3, $p = 0.246$; zone 4, $p = 0.082$; paired t-test). Note that retinal eccentricity is not considered a variable because the independent retinal locations were from the same region of retina (see Fig. 1). (B) Proportion each zone contributes to the total retinal thinning as measured with OCT and calculated with Eq. (2). (C) Proportion each zone contributes to the total retinal thinning as measured with histology and calculated with Eq. (2). Zones 2 and 3 contribute the most to total thinning for both OCT (zone 1/2, $p = 0.001$; zone 1/3, $p = 0.020$; zone 1/4, $p = 0.139$; zone 2/3, $p = 0.076$; zone 2/4, $p < 0.001$; zone 3/4, $p = 0.006$; paired t-test) and histology (zone 1/2, $p = 0.003$; zone 1/3, $p = 0.230$; zone 1/4, $p = 0.742$; zone 2/3, $p = 0.113$; zone 2/4, $p < 0.001$; zone 3/4, $p < 0.001$; paired t-test) methods of measurement. *represents $p < 0.05$.

4.2. Total retinal thinning in high myopia

Retinal thinning in myopia has been demonstrated with OCT analysis in human studies (Choi & Lee, 2006; Lam et al., 2007; Leung et al., 2006; Liew et al., 2007; Lim et al., 2005; Luo et al., 2006; Wolsley et al., 2008; Wu et al., 2008), and also with histology analysis in various species (Curtin, 1985; McBrien et al., 1995; Yanoff & Fine, 2002; Yinon, Koslowe, Lobel, Landshman, & Barishak, 1982; Zhou et al., 2010). The most recent OCT studies in human have determined that the macula generally flattens in myopia by thinning at the perifovea and thickening at the foveal pit (Lam et al., 2007; Lim et al., 2005; Wolsley et al., 2008; Wu et al., 2008). However, earlier studies found either foveal thinning (Mrugacz, Bakunowicz-Lazarczyk, & Sredzinska-Kita, 2004) or no difference in foveal thickness (Choi & Lee, 2006; Wakitani et al., 2003). These measurements at the macular region are not directly comparable to our results in the superior nasal quadrant, as the macula is a structurally specialized region of the retina. In this study, retinas from myopic eyes (mean −15.9 D) showed comparable mean thinning of 15 ± 5% (32 μm) with the OCT method and 17 ± 3% (24 μm) with the histology method (Fig. 5A) in the superior nasal quadrant. The absolute values of retinal thickness measured by the histological method are smaller than the values measured by OCT, due to shrinkage during dehydration (Abbott et al., 2009). The percentage of retinal thinning (15–17%) is just over half the percentage of mean vitreous chamber elongation (28 ± 7%). The similarity between the results from OCT and histology methods validates OCT as a useful tool for *in vivo* measuring and monitoring of retinal thickness changes in myopia.

4.3. Differential thinning of retinal layers in high myopia

A new finding from this study is that zones 2 and 3, representing the inner plexiform, inner nuclear and outer plexiform layers, contribute the most to total retinal thinning in axial myopia (approximately 35% and 30% of total thinning respectively). Zone 4, representing the photoreceptors and retinal pigment epithelium, contributes the least to total retinal thinning in myopia (approximately 15% of total thinning). Zone 1, representing the nerve fiber and ganglion cell layers, contributes approximately 20% to the total thinning. This result is consistent with findings from an OCT study in human, which suggested thinning occurs more in the middle to inner retina (encompassing the ganglion cell, inner plexiform, inner nuclear and outer plexiform layers) (Wolsley et al., 2008). Thus it seems that the inherently thicker retinal layers are more susceptible or adaptable to the effects of mechanical or biochemical changes in myopia. Since retinal stretch slowly increases as myopia develops, cell connections in the plexiform layers may be able to anatomically adapt. For example, previous studies have shown that amacrine and ganglion cell dendrites are able to elongate in myopia (Teakle, Wildsoet, & Vaney, 1993; Troilo, Xiong, Crowley, & Finlay, 1996).

4.4. Mechanism of retinal thinning in axial myopia

In the present study, there was a decrease in areal density for all cell types except Müller cells, suggesting that photoreceptors, bipolar/horizontal cells, amacrine cells and ganglion cells all contribute to retinal thinning. Previous studies using a variety of approaches including psychophysics (Chui, Yap, Chan, & Thibos, 2005; Jaworski, Gentle, Zele, Vingrys, & McBrien, 2006), histological cell counts (Grossniklaus & Green, 1992), and adaptive optics imaging of the cone mosaic (Chui, Song, & Burns, 2008; Kitaguchi et al., 2007; Li, Tiruveedhula, & Roorda, 2010) all find evidence of decreased photoreceptor density in eyes with increased axial length. Most of these studies suggest that tangential retinal stretch (Wu et al., 2008) plays a significant role in the amount of retinal thinning in myopia. It is possible that photoreceptor apoptosis also contributes (Mao, Liu, Wen, Tan, & Fu, 2006; Xu, Li, & Tso, 1996).

The volumetric cell density data presented in this study shows that the cell number to volume ratio remains equivalent between myopic and control eyes. This is a new finding that will help with determining the proportion (if any) of cell loss in future studies. A study that accurately measures the surface area and the variable thickness of the entire retina to directly estimate the total retinal volume is required. Since the volumetric density is equivalent in the retina of myopic and emmetropic eyes, the relative change in cell number in myopia can then be determined.

4.5. Regional variation of retinal thinning in high myopia

As suggested by Li et al. (2010) and Wolsley et al. (2008), it seems likely that retinal stretch causes differential effects on specialized regions of the retina. A comprehensive study of the variation in thinning at different retinal eccentricities is yet to be reported. Wolsley et al. (2008) shows retinal thinning measured with OCT in human

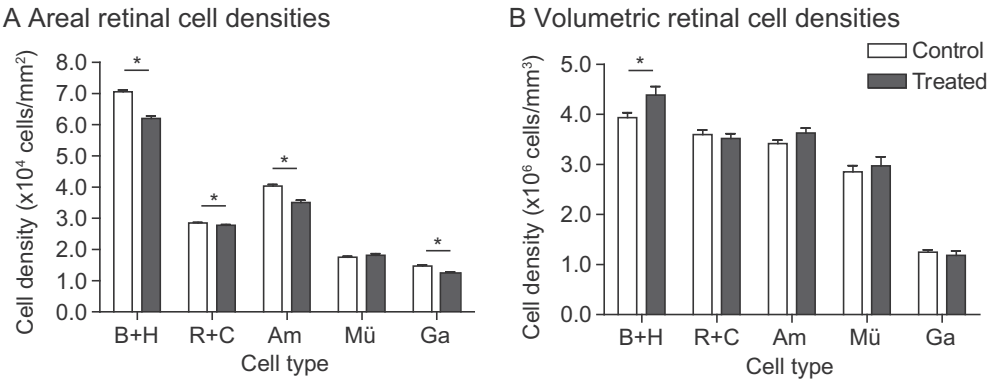

Fig. 6. Cell densities (mean ± SEM) in the treated and control eye of one tree shrew (TS1) at a region (size 560 × 560 μm) located 2.7 mm from the center of the optic disc in the superior nasal quadrant (n = 12 vertical sections per eye). (A) Areal cell densities expressed as the number of cells per mm^2 for five groups of cells; bipolar and horizontal cells (B + H), rods and cones (R + C), amacrine cells (Am), Müller cells (Mü), ganglion cells and displaced amacrine cells (Ga). For all cell types apart from Müller cells (p = 0.292; unpaired t-test), there are greater cell densities in the control eye than the treated eye (bipolar and horizontal cells, p < 0.001; rods and cones, p = 0.033; amacrine cells, p < 0.001; ganglion cells, p < 0.001; unpaired t-test). (B) Volumetric cell densities expressed as the number of cells per mm^3 for the same five groups as in A. The volumetric cell densities in the treated eye are generally comparable to that in the control eye (rods and cones, p = 0.555; amacrine cells, p = 0.086; Müller cells, p = 0.581; ganglion cells, p = 0.542; unpaired t-test) except for the bipolar and horizontal cell group (p = 0.028; unpaired t-test). *represents p < 0.05.

myopes compared to emmetropes along a line from 16° superior temporal to the fovea to 16° inferior nasal. The thinning appeared to slowly increase from 4° to 16° nasally and temporally, but regional differences were not analyzed in detail. The initial OCT analysis in the present study suggests that nasal retina (up to 18° from the center of the optic disc) is thinner than the corresponding temporal retina. In tree shrew the area centralis is approximately 31° from the disc (calculated from retinal maps in DeBruyn (1983)), while in human the fovea is approximately 15° from the disc. Further systematic investigation of eccentricity changes in retinal thinning relative to both the disc and the fovea are required.

5. Conclusions

The thickness of the retina in highly myopic eyes was reduced by 15–17%. The percentage of retinal thinning was comparable between *in vivo* (OCT) and *in vitro* (histological) methods. Retinal thinning varied across layers, with 35% of the thinning occurring in the inner plexiform layer, 30% in the inner nuclear and outer plexiform layers, 20% in the nerve fiber and ganglion cell layers, and 15% in the photoreceptor layer and retinal pigment epithelium. Cell density analysis showed that all neuronal cell types are involved in retinal thinning. Future work could use this mammalian model of axial myopia combined with noninvasive measurements of retinal thickness using OCT to determine the time course of retinal thinning and the correlation between retinal thinning, axial elongation and ensuing chorioretinal pathology.

Acknowledgments

The authors would like to acknowledge and thank Paul Martin for his assistance with the cell density measurements and analysis, Erica Fletcher for discussion on retinal morphology changes, and Paul Fijn for statistical advice.

This work was supported by National Health and Medical Research Council of Australia Grants #255157 and #454602 to N.M^{c}B., a Retina Australia Grant to M.J.P., a Lions Vision Research Fellowship to U.G. and an Ernst and Grace Matthaei Scholarship to C.J.A.

References

Abbott, C. J., McBrien, N. A., Grünert, U., & Pianta, M. J. (2009). Relationship of the optical coherence tomography signal to underlying retinal histology in the tree shrew (*Tupaia belangeri*). *Investigative Ophthalmology and Visual Science, 50*(1), 414–423.

Adams, C. K., Perez, J. M., & Hawthorne, M. N. (1974). Rod and cone densities in the *Rhesus*. *Investigative Ophthalmology and Visual Science, 13*(11), 885–888.

Anger, E. M., Unterhuber, A., Hermann, B., Sattmann, H., Schubert, C., Morgan, J. E., et al. (2004). Ultrahigh resolution optical coherence tomography of the monkey fovea. Identification of retinal sublayers by correlation with semithin histology sections. *Experimental Eye Research, 78*(6), 1117–1125.

Cao, Q. L., Murphy, H. A., & Petry, H. M. (1999). Localization of nitric oxide synthase in the tree shrew retina. *Visual Neuroscience, 16*(3), 399–409.

Celorio, J. M., & Pruett, R. C. (1991). Prevalence of lattice degeneration and its relation to axial length in severe myopia. *American Journal of Ophthalmology, 111*(1), 20–23.

Chiang, L. M., Ho, T. C., Lin, L. L., Yang, C. M., Liu, K. R., & Chen, M. S. (1993). Prevalence of retinal detachment and peripheral retinal degeneration in high myopia college students in Taiwan. *Investigative Ophthalmology and Visual Science, 34*, S937.

Choi, S. W., & Lee, S. J. (2006). Thickness changes in the fovea and peripapillary retinal nerve fiber layer depend on the degree of myopia. *Korean Journal of Ophthalmology, 20*(4), 215–219.

Chui, T. Y., Song, H., & Burns, S. A. (2008). Individual variations in human cone photoreceptor packing density: Variations with refractive error. *Investigative Ophthalmology and Visual Science, 49*(10), 4679–4687.

Chui, T. Y., Yap, M. K., Chan, H. H., & Thibos, L. N. (2005). Retinal stretching limits peripheral visual acuity in myopia. *Vision Research, 45*(5), 593–605.

Curcio, C. A., Packer, O., & Kalina, R. E. (1987). A whole mount method for sequential analysis of photoreceptor and ganglion cell topography in a single retina. *Vision Research, 27*(1), 9–15.

Curtin, B. J. (1985). *The myopias: Basic science and clinical management*. Philadelphia: Harper & Row.

Curtin, B. J., & Karlin, D. B. (1971). Axial length measurements and fundus changes of the myopic eye. *American Journal of Ophthalmology, 71*(1), 42–53.

David, T., Smye, S., Dabbs, T., & James, T. (1998). A model for the fluid motion of vitreous humour of the human eye during saccadic movement. *Physics in Medicine and Biology, 43*(6), 1385–1399.

DeBruyn, E. J. I. (1983). The organization and central terminations of retinal ganglion cells in the tree shrew (*Tupaia glis*). In *Anatomy*. Nashville: Vanderbilt University.

Fledelius, H. C. (1988). Myopia prevalence in Scandinavia. A survey, with emphasis on factors of relevance for epidemiological refraction studies in general. *Acta Ophthalmologica Supplementum, 185*, 44–50.

Ge, J., Luo, R., & Guo, Y. (1999). Corrective change of retinal thickness measured by optical coherence tomography and histologic studies. *Yan Ke Xue Bao, 15*(3). 153–155, 178.

Goh, W. S., & Lam, C. S. (1994). Changes in refractive trends and optical components of Hong Kong Chinese aged 19–39 years. *Ophthalmic and Physiological Optics, 14*(4), 378–382.

Goodchild, A. K., & Martin, P. R. (1998). The distribution of calcium-binding proteins in the lateral geniculate nucleus and visual cortex of a New World monkey, the marmoset, *Callithrix jacchus*. *Visual Neuroscience, 15*(4), 625–642.

Grey, R. H., Burns-Cox, C. J., & Hughes, A. (1989). Blind and partial sight registration in Avon. *British Journal of Ophthalmology, 73*(2), 88–94.

Grossniklaus, H. E., & Green, W. R. (1992). Pathologic findings in pathologic myopia. *Retina, 12*(2), 127–133.

Halasz, P., & Martin, P. R. (1984). A microcomputer based system for semi-automatic analysis of histological sections. *Proceedings of the Royal Microscopical Society, 19*, 312.

Hee, M. R., Izatt, J. A., Swanson, E. A., Huang, D., Schuman, J. S., Lin, C. P., et al. (1995). Optical coherence tomography of the human retina. *Archives of Ophthalmology, 113*(3), 325–332.

Huang, D., Swanson, E. A., et al. (1991). Optical coherence tomography. *Science, 254*(5035), 1178–1181.

Jaworski, A., Gentle, A., Zele, A. J., Vingrys, A. J., & McBrien, N. A. (2006). Altered visual sensitivity in axial high myopia: A local postreceptoral phenomenon? *Investigative Ophthalmology and Visual Science, 47*(8), 3695–3702.

Kempen, J. H., Mitchell, P., Lee, K. E., Tielsch, J. M., Broman, A. T., Taylor, H. R., et al. (2004). The prevalence of refractive errors among adults in the United States, Western Europe, and Australia. *Archives of Ophthalmology, 122*(4), 495–505.

Kitaguchi, Y., Bessho, K., Yamaguchi, T., Nakazawa, N., Mihashi, T., & Fujikado, T. (2007). In vivo measurements of cone photoreceptor spacing in myopic eyes from images obtained by an adaptive optics fundus camera. *Japan Journal of Ophthalmology, 51*(6), 456–461.

Kolb, H., & Wang, H. H. (1985). The distribution of photoreceptors, dopaminergic amacrine cells and ganglion cells in the retina of the North American opossum (*Didelphis virginiana*). *Vision Research, 25*(9), 1207–1221.

Kremser, B., Troger, J., Baltaci, M., Kralinger, M., & Kieselbach, G. F. (1999). Retinal thickness analysis in subjects with different refractive conditions. *Ophthalmologica, 214*(6), 376–379.

Lam, D. S., Leung, K. S., Mohamed, S., Chan, W. M., Palanivelu, M. S., Cheung, C. Y., et al. (2007). Regional variations in the relationship between macular thickness measurements and myopia. *Investigative Ophthalmology and Visual Science, 48*(1), 376–382.

Leung, C. K., Mohamed, S., et al. (2006). Retinal nerve fiber layer measurements in myopia: An optical coherence tomography study. *Investigative Ophthalmology and Visual Science, 47*(12), 5171–5176.

Li, K. Y., Tiruveedhula, P., & Roorda, A. (2010). Inter-subject variability of foveal cone photoreceptor density in relation to eye length. *Investigative Ophthalmology and Visual Science*. doi:10.1167/iovs.10-5499.

Liew, S. H., Gilbert, C. E., Spector, T. D., Marshall, J., & Hammond, C. J. (2007). The role of heredity in determining central retinal thickness. *British Journal of Ophthalmology, 91*(9), 1143–1147.

Lim, M. C., Hoh, S. T., Foster, P. J., Lim, T. H., Chew, S. J., Seah, S. K., et al. (2005). Use of optical coherence tomography to assess variations in macular retinal thickness in myopia. *Investigative Ophthalmology and Visual Science, 46*(3), 974–978.

Lin, L. L., Shih, Y. F., Tsai, C. B., Chen, C. J., Lee, L. A., Hung, P. T., et al. (1999). Epidemiologic study of ocular refraction among schoolchildren in Taiwan in 1995. *Optometry and Vision Science, 76*(5), 275–281.

Luo, H. D., Gazzard, G., et al. (2006). Myopia, axial length, and OCT characteristics of the macula in Singaporean children. *Investigative Ophthalmology and Visual Science, 47*(7), 2773–2781.

Mao, J., Liu, S., Wen, D., Tan, X., & Fu, C. (2006). Basic fibroblast growth factor suppresses retinal neuronal apoptosis in form-deprivation myopia in chicks. *Current Eye Research, 31*(11), 983–987.

Marsh-Tootle, W. L., & Norton, T. T. (1989). Refractive and structural measures of lid-suture myopia in tree shrew. *Investigative Ophthalmology and Visual Science, 30*(10), 2245–2257.

Maruo, T., Ikebukuro, N., Kawanabe, K., & Kubota, N. (1991). Changes in causes of visual handicaps in Tokyo. *Japanese Journal of Ophthalmology, 35*(3), 268–272.

McBrien, N. A., & Gentle, A. (2003). Role of the sclera in the development and pathological complications of myopia. *Progress in Retinal and Eye Research, 22*(3), 307–338.

McBrien, N. A., Moghaddam, H. O., Cottriall, C. L., Leech, E. M., & Cornell, L. M. (1995). The effects of blockade of retinal cell action potentials on ocular growth,

emmetropization and form deprivation myopia in young chicks. *Vision Research, 35*(9), 1141–1152.
McBrien, N. A., Moghaddam, H. O., & Reeder, A. P. (1993). Atropine reduces experimental myopia and eye enlargement via a nonaccommodative mechanism. *Investigative Ophthalmology and Visual Science, 34*(1), 205–215.
McBrien, N. A., & Norton, T. T. (1992). The development of experimental myopia and ocular component dimensions in monocularly lid-sutured tree shrews (*Tupaia belangeri*). *Vision Research, 32*(5), 843–852.
Metlapally, S., & McBrien, N. A. (2008). The effect of positive lens defocus on ocular growth and emmetropization in the tree shrew. *Journal of Vision, 8*(3), 11–12.
Mrugacz, M., Bakunowicz-Lazarczyk, A., & Sredzinska-Kita, D. (2004). Use of optical coherence tomography in myopia. *Journal of Pediatric Ophthalmology and Strabismus, 41*, 159–162.
Norton, T. T., & McBrien, N. A. (1992). Normal development of refractive state and ocular component dimensions in the tree shrew (*Tupaia belangeri*). *Vision Research, 32*(5), 833–842.
Ochs, M., Mayhew, T. M., & Knabe, W. (2000). To what extent are the retinal capillaries ensheathed by Müller cells? A stereological study in the tree shrew *Tupaia belangeri*. *Journal of Anatomy, 196*(Pt 3), 453–461.
Ogden, T. E. (1975). The receptor mosaic of *Aotes trivirgatus*: Distribution of rods and cones. *Journal of Comparative Neurology, 163*(2), 193–202.
Perry, V. H., & Cowey, A. (1985). The ganglion cell and cone distributions in the monkey's retina: Implications for central magnification factors. *Vision Research, 25*(12), 1795–1810.
Reichenbach, A., Fromter, C., Engelmann, R., Wolburg, H., Kasper, M., & Schnitzer, J. (1995). Müller glial cells of the tree shrew retina. *Journal of Comparative Neurology, 360*, 257–270.
Reymond, L. (1985). Spatial visual acuity of the eagle *Aquila audax*: A behavioural, optical and anatomical investigation. *Vision Research, 25*(10), 1477–1491.
Rose, R. D., & Rohrlich, D. (1988). Counting sectioned cells via mathematical reconstruction. *Journal of Comparative Neurology, 272*(4), 365–386.
Rosenberg, T., & Klie, F. (1996). Current trends in newly registered blindness in Denmark. *Acta Ophthalmologica Scandinavica, 74*(4), 395–398.
Sherman, S. M., Norton, T. T., & Casagrande, V. A. (1977). Myopia in the lid-sutured tree shrew (*Tupaia glis*). *Brain Research, 124*(1), 154–157.
Siegwart, J. T., Jr., & Norton, T. T. (1994). Goggles for controlling the visual environment of small animals. *Laboratory Animal Science, 44*(3), 292–294.
Steinberg, R. H., Reid, M., & Lacy, P. L. (1973). The distribution of rods and cones in the retina of the cat (*Felis domesticus*). *Journal of Comparative Neurology, 148*(2), 229–248.
Teakle, E. M., Wildsoet, C. F., & Vaney, D. I. (1993). The spatial organization of tyrosine hydroxylase-immunoreactive amacrine cells in the chicken retina and the consequences of myopia. *Vision Research, 33*(17), 2383–2396.
Tokoro, T. (1998). *Atlas of posterior fundus changes in pathologic myopia*. Tokyo: Springer-Verlag.
Troilo, D., Xiong, M., Crowley, J. C., & Finlay, B. L. (1996). Factors controlling the dendritic arborization of retinal ganglion cells. *Visual Neuroscience, 13*(4), 721–733.
Vitale, S., Sperduto, R. D., & Ferris, F. L. 3rd, (2009). Increased prevalence of myopia in the United States between 1971–1972 and 1999–2004. *Archives of Ophthalmology, 127*(12), 1632–1639.
Wakitani, Y., Sasoh, M., Sugimoto, M., Ito, Y., Ido, M., & Uji, Y. (2003). Macular thickness measurements in healthy subjects with different axial lengths using optical coherence tomography. *Retina, 23*(2), 177–182.
Wensor, M., McCarty, C. A., & Taylor, H. R. (1999). Prevalence and risk factors of myopia in Victoria, Australia. *Archives of Ophthalmology, 117*(5), 658–663.
Wilder, H. D., Grünert, U., Lee, B. B., & Martin, P. R. (1996). Topography of ganglion cells and photoreceptors in the retina of a New World monkey: The marmoset *Callithrix jacchus*. *Visual Neuroscience, 13*, 335–352.
Wolsley, C. J., Saunders, K. J., Silvestri, G., & Anderson, R. S. (2008). Investigation of changes in the myopic retina using multifocal electroretinograms, optical coherence tomography and peripheral resolution acuity. *Vision Research, 48*(14), 1554–1561.
Wu, P. C., Chen, Y. J., Chen, C. H., Chen, Y. H., Shin, S. J., Yang, H. J., et al. (2008). Assessment of macular retinal thickness and volume in normal eyes and highly myopic eyes with third-generation optical coherence tomography. *Eye, 22*(4), 551–555.
Wu, H. M., Seet, B., Yap, E. P., Saw, S. M., Lim, T. H., & Chia, K. S. (2001). Does education explain ethnic differences in myopia prevalence? A population-based study of young adult males in Singapore. *Optometry and Vision Science, 78*(4), 234–239.
Xu, G. Z., Li, W. W., & Tso, M. O. (1996). Apoptosis in human retinal degenerations. *Transactions of the American Ophthalmological Society, 94*, 411–430.
Yannuzzi, L. A., Sorenson, J. A., et al. (1993). Risk factors for idiopathic rhegmatogenous retinal detachment. The Eye Disease Case-Control Study Group. *American Journal of Epidemiology, 137*(7), 749–757.
Yanoff, M., & Fine, B. S. (2002). *Ocular pathology* (5th ed). St. Louis: Mosby.
Yinon, U., Koslowe, K. C., Lobel, D., Landshman, N., & Barishak, Y. R. (1982). Lid suture myopia in developing chicks: Optical and structural considerations. *Current Eye Research, 2*(12), 877–882.
Zhou, X., An, J., Wu, X., Lu, R., Huang, Q., Xie, R., et al. (2010). Relative axial myopia induced by prolonged light exposure in C57BL/6 mice. *Photochemistry and Photobiology, 86*(1), 131–137.